

## Spheromak Formation by Steady Inductive Helicity Injection

T. R. Jarboe, C. Akcay, W. T. Hamp, R. Z. Aboul Hosn, G. J. Marklin, B. A. Nelson, R. G. O'Neill, P. E. Sieck, R. J. Smith, and J. S. Wrobel

University of Washington, Seattle, WA, 98195-2250.

Email: [Jarboe@aa.washington.edu](mailto:Jarboe@aa.washington.edu)

**Abstract.** Since the last IAEA meeting, new understanding and parameters have been achieved on the Helicity Injected Torus with Steady Inductive helicity injection current drive (HIT-SI) experiment. The Taylor-state model is shown to agree with HIT-SI surface and internal magnetic profile measurements. Helicity balance predicts the peak magnitude of toroidal spheromak current and the threshold for spheromak formation. The model also confirms that the injector loop voltage is consistent with the spheromak being maintained by helicity injection from the insulated walls of the spheromak and not from the injectors. Spheromaks with currents up to 29 kA have been produced.

### 1. Introduction and Taylor Model Agreement with Equilibrium

Helicity injection current drive relies on helicity-conserving relaxation towards the minimum energy state, which satisfies  $\nabla \times \mathbf{B} = \lambda \mathbf{B}$ , where  $\lambda (= \mu_0 j / B)$  is a global constant. As the helicity is increased with fixed geometry and flux boundary conditions  $\lambda$  increases until it reaches the value of the lowest eigenstate. The eigenstate fits the geometry with no flux linking or penetrating the boundary and, as the helicity is increased further,  $j$  and  $B$  increase together at the constant  $\lambda_{\text{sph}}$  value of the eigenstate [1]. In a normal RFP the lowest eigenstate is an  $m = 1$  helical structure and it has not been clearly observed, although, it is related to the  $m = 1$  kink mode observed at high  $\lambda$ . In HIT-SI the lowest eigenstate is the spheromak equilibrium and it is clearly observed [2]. The experiment has a bowtie shaped spheromak confinement region with two helicity injectors. The inductive injectors are  $180^\circ$  segments of a small, oval-cross-section RFP. In each injector the loop voltage and toroidal flux are oscillated in phase at 5.8 kHz. See Figure 1. The injectors are  $90^\circ$  out of phase with each other but have the same amplitude of voltage ( $V_o$ ) and flux ( $\psi_o$ ). This gives a constant helicity injection rate of  $2V_o\psi_o$ . A more complete description of the machine is given elsewhere [3,4]. If the helicity content is high enough to form a spheromak, the true Taylor state of HIT-SI has three components: Two mostly  $n = 1$  odd components, one from each injector with their flux having just enough current so that  $\lambda_{\text{inj}}$  in each is  $\lambda_{\text{sph}}$ , and a spheromak component that has the amplitude needed to contain the remaining helicity [2]. This superposition of Taylor states is still a Taylor-state equilibrium since  $\lambda$  is the same for all states in the superposition. By adding the spheromak state to the injector states, Taylor states with any ratio of injector currents to spheromak current can be calculated. Figure 2 [5] shows the injector parameters. Surface probe and flux loop locations are shown in Figure 1. They are imbedded in the copper flux conserver to minimize plasma perturbations. Their frequency dependent sensitivity is calibrated by imposing a known amplitude and frequency of magnetic field on the surface and measuring their response. Figures 3-6 show surface and internal magnetic field data compared to the Taylor state [5]. The agreement is remarkable. The toroidal currents in each injector and the spheromak uniquely define the Taylor state. The injector currents are measured directly with a Rogowski loop.

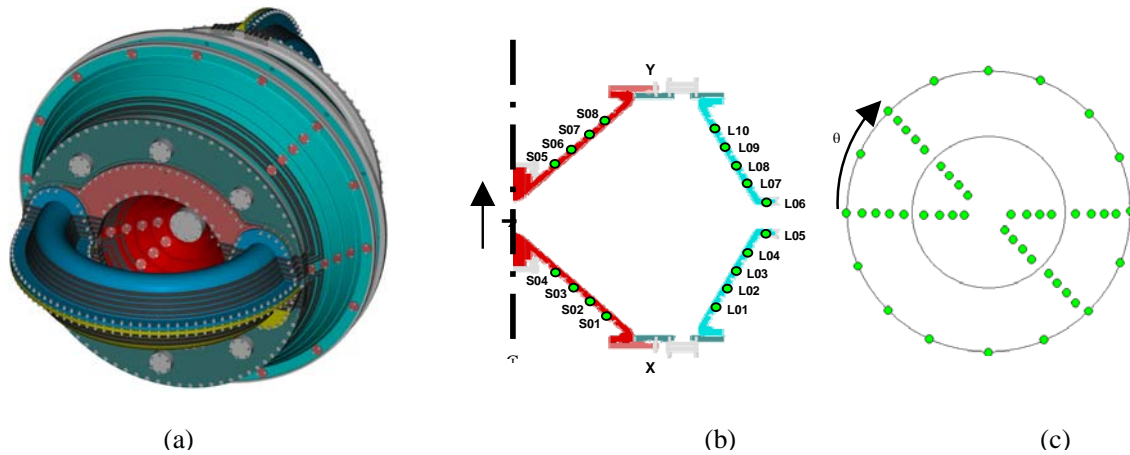


Figure 1. (a) an assembly drawing showing the copper shell and air core transformer windings (b) poloidal location of surface probes and their label; toroidal flux loops are located in the notches between the probes. (c) toroidal location of surface probes. For example, a surface probe labeled LO1P000 is at poloidal location L01, measuring poloidal field ( $T$  is used for toroidal), and is at  $\theta = 0$  degrees.

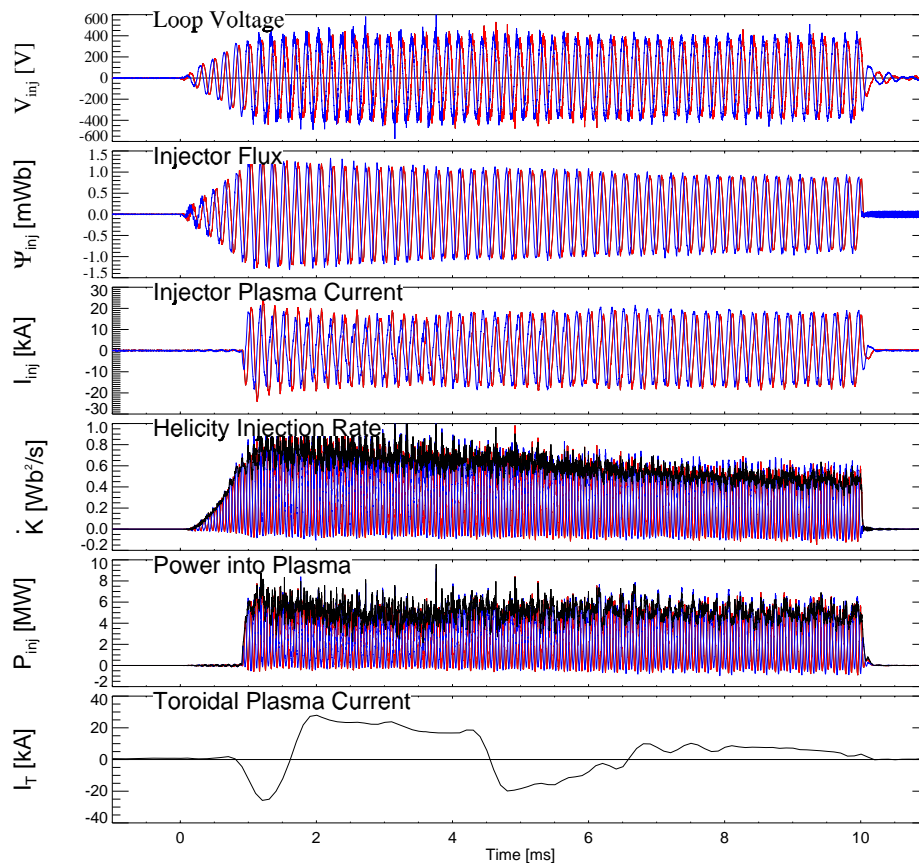


Figure 2. Injector parameters and spheromak toroidal current for HIT-SI shot #105278. Red traces represent the X injector, and blue traces represent the Y injector. The black traces on the helicity injection rate and power input plots are the sum of the two injectors. The slow decay and flipping of the spheromak are not understood at this time.

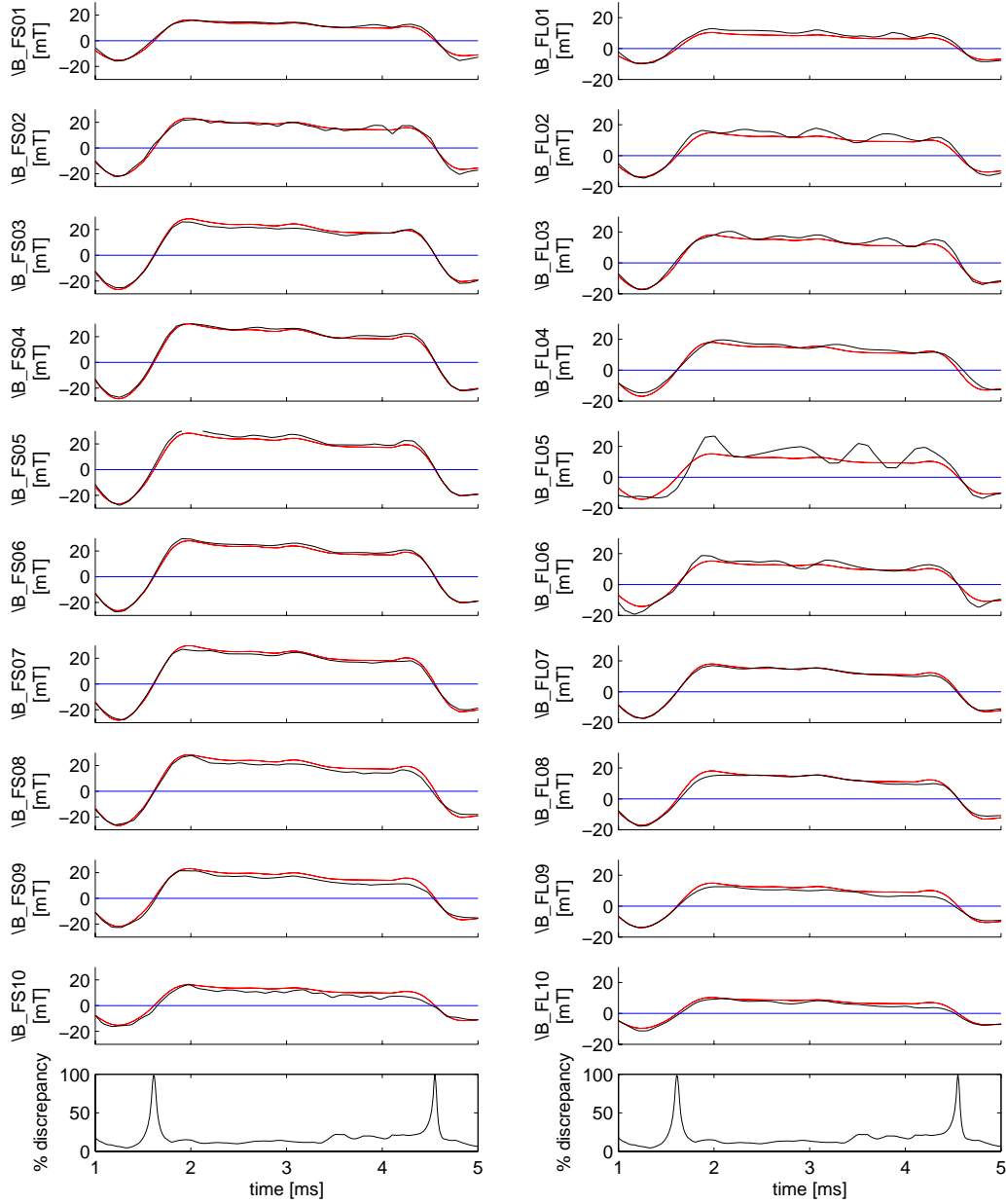


Figure 3. Toroidally-averaged poloidal fields from the flux loops and the fit from the Taylor model for shot 105278. The flux loops are located in the notches between the probe locations shown in Figure 1b. Field measurements are in black; the model fit is in red. The flux loops are shielded from the plasma by 6 mm of copper and are insensitive to the 5.8 kHz injector generated fields.

The toroidal spheromak current is found by fitting to the flux loop data shown in Figure 3. Thus, there is only a single time dependent fitting parameter. The discrepancy is defined as:

$$\text{discrepancy} = \frac{1}{N} \sum_N \frac{|B_{\text{model}} - B_{\text{measured}}|}{|B_{\text{measured}}|}$$

where N is the number of data traces in the column presented.

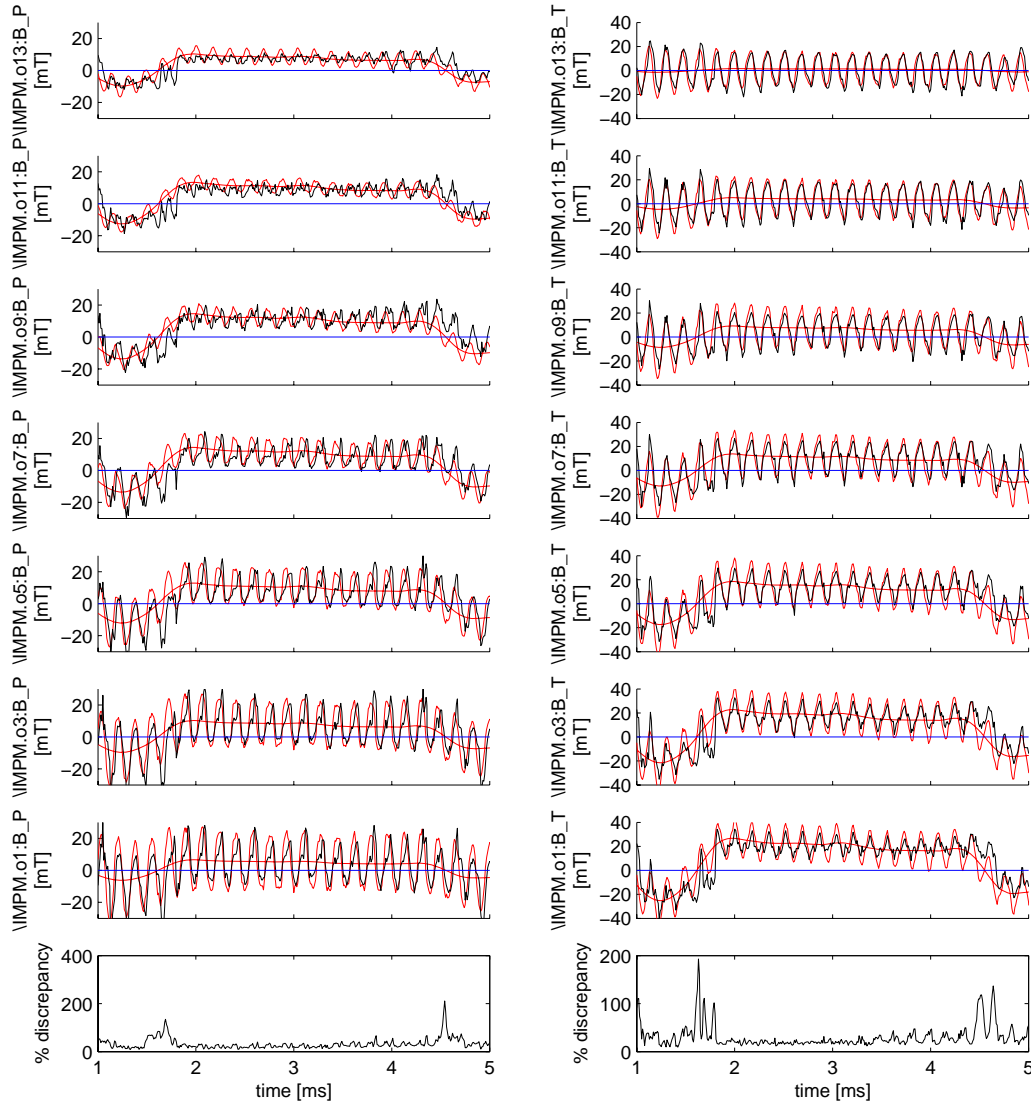


Figure 4. Measurements from the internal magnetic field probes and the prediction from the Taylor model for shot 105278. Field measurements are in black; the model fit is in red. The slowly-varying spheromak component of the model is also plotted in red. Probe 1 (bottom) is the deepest at  $R=0.36$  m; probe 13 (top) is at the edge at  $R=0.52$  m. Poloidal fields are plotted at left, toroidal at right. Observe the unidirectional poloidal field at the wall and unidirectional toroidal field at  $R=0.36$  m.

Both the surface fields and internal field profile agree to within 10% of the fields measured in the experiment, using only the spheromak current as the fitting parameter. The smooth red trace shows the spheromak field. Analysis of the Taylor state shows that some closed flux surfaces are formed that do not link the injectors when the spheromak toroidal current equals or exceeds the amplitude of the injector currents [2]. Injector current amplitudes of 20 kA were used to produce the 29 kA spheromak.

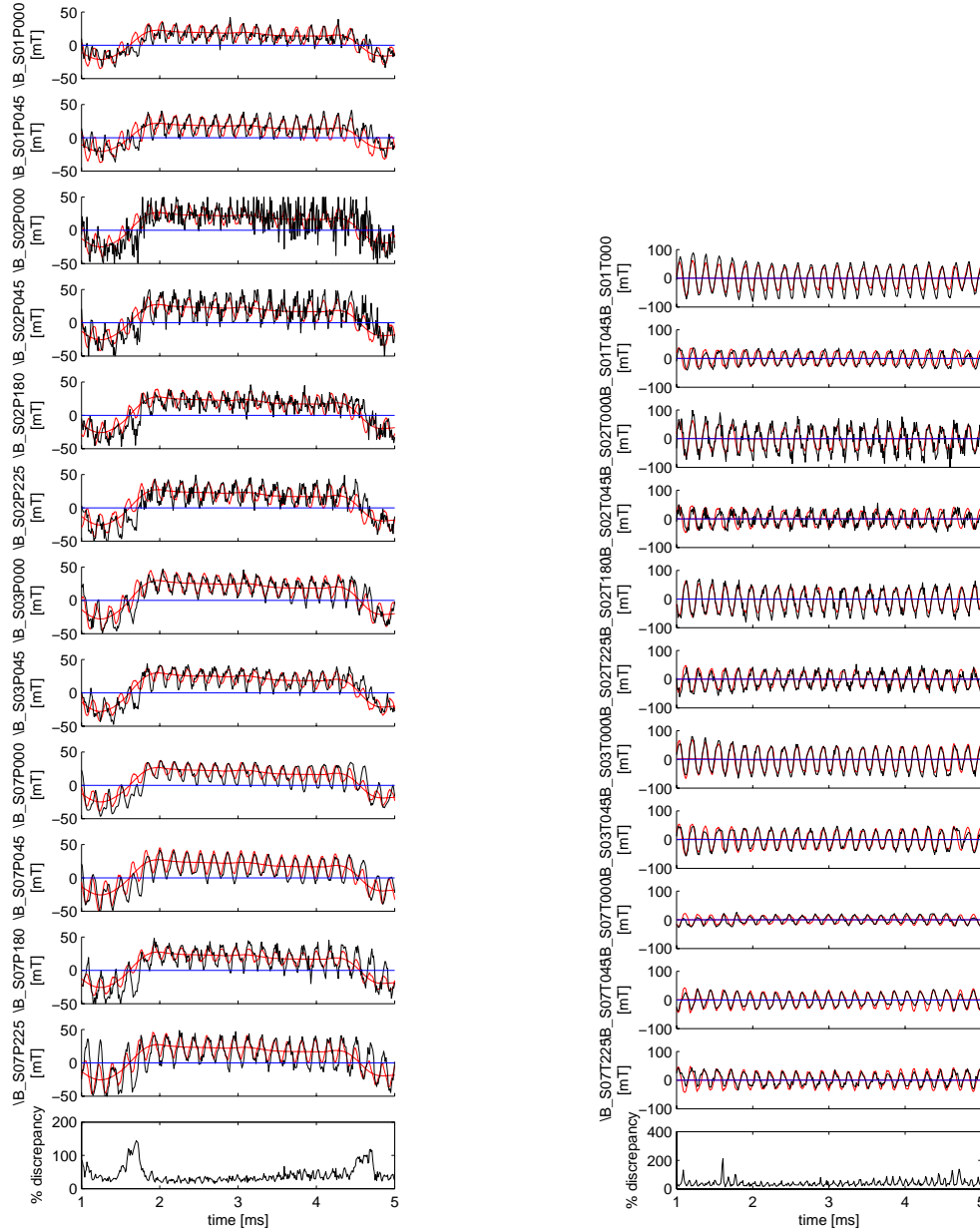


Figure 5. Measurements from the small cone surface field probes and the prediction from the Taylor model for shot 105278. Field measurements are in black; the model fit is in red. The slowly-varying spheromak component of the model is also plotted in red. Poloidal fields are plotted at left, toroidal at right. The spheromak component has zero toroidal field at the surface of the flux conserver. So the toroidal field at the surface is due to the injector components and the Taylor model predicts their values very accurately. The  $n = 1$  variation of the toroidal field at the wall reflexes the  $n = 1$  nature of the injectors.

## 2. Helicity Balance Model and Agreement with Data

By assuming helicity is injected at a rate  $2V_0\psi_0$ , and only decays through resistivity, the equilibrium is predicted with no fitting parameters, demonstrating helicity balance in a sustained spheromak for the first time without the large uncertainty of electrode sheath drops [6]. Spitzer resistivity (using  $Z=2$ ) is assumed, with the electron temperature measured by

Langmuir probe. Although the experimental results, at the time of peak current, suggest a higher effective resistivity by a factor of 1.5 compared to the Spitzer value the prediction is

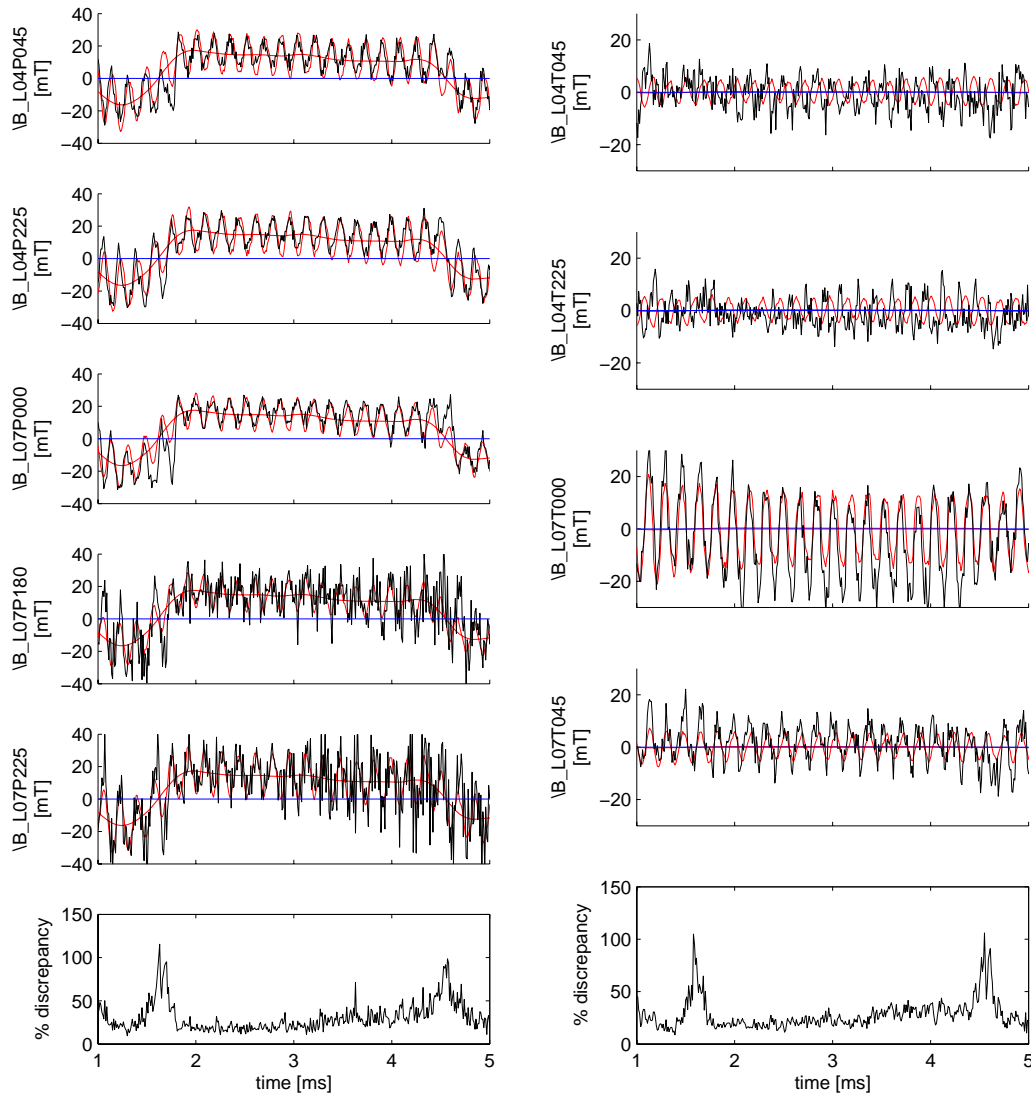


Figure 6. Measurements from the large cone surface field probes and the prediction from the Taylor model for shot 105278. Field measurements are in black; the model fit is in red. The slowly-varying spheromak component of the model is plotted in red. Poloidal fields are on the left, toroidal at right.

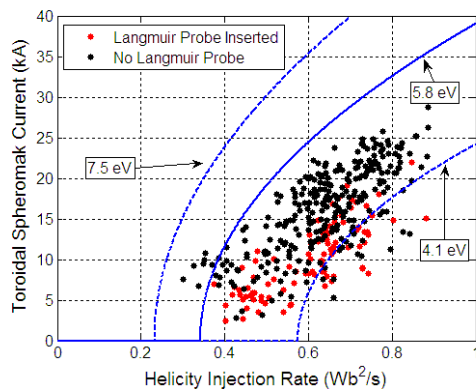


Figure 7. Peak spheromak current versus helicity injection rate.

still within the uncertainties in the measured parameters. In Figure 7, the points are the peak current of the discharge for the given helicity injection rate. The solid blue curve is predicted by the model using the measured 5.8 eV temperature. The dashed curves show the uncertainty in the prediction due to uncertainties in the temperature data. The low temperatures are due to a carbon radiation barrier. The carbon is from an insulator arcing problem that has been addressed.

The decrease in time of the sustained spheromak current is not understood at this time but may be related to a slowly growing  $n = 2$  locked mode. The lowest eigenstate has even symmetry and is mostly  $n = 0$ . However, it does have a small  $n = 2$  component due to the injector openings in the flux conserver which grow in time due to magnetic diffusion into the flux conserver. The flux conserver is being improved to increase the decay time of the  $n = 2$  component.

### 3. Location of Helicity Injection

The entire inside of the copper shell shown in Figure 1a is coated with 0.3 mm of alumina so the shell cannot act as an electrode. Thus, the loop voltage is distributed on the plasma side of the insulator consistent with the plasma impedance. Langmuir probes placed where the injectors connect to the spheromak region are used to determine the loop voltage division between the injector region and the spheromak region [7]. Four probe tips are placed in each opening of the x-injector. The voltage differences between the probes are measured and the voltage from the edge probe to the copper shell is also measured. Since the sheath drops cancel on this voltage measurement the simple floating potentials are used. The voltage drop in the spheromak and in the injector regions is determined from the measurements. Figure 8 [7] shows the drop in the spheromak region. The dominant voltage drop is from the shell to the edge probe with little 5.8 kHz voltage measured between the probes. Most of the large

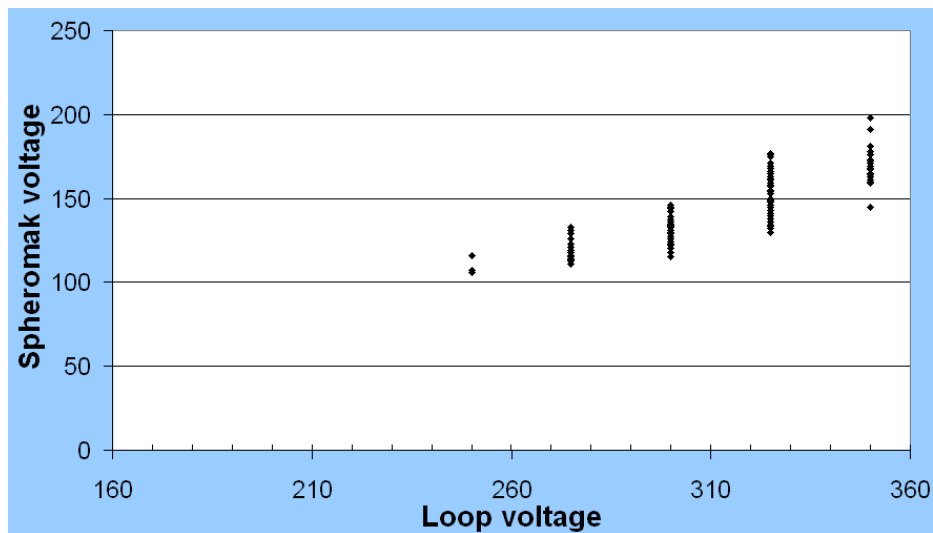


Figure 8. Spheromak voltage drop versus the total applied loop voltage. As the loop voltage is increased above the breakdown threshold most of the increase is applied to the spheromak.

edge voltage is probably also across the insulator with low electric field in the plasma. Thus, the low electric field in the injector opening indicates that power and helicity are not flowing from the injector to the spheromak but flowing into the spheromak from the insulating walls of the spheromak region. This is further confirmed by the observation that the injector voltage drop is consistent with only that needed to maintain the helicity in the injector. See Figure 9 [8]. The voltage division between injector and spheromak regions is found to agree with that required to maintain the injector helicity to within 20%. This is also consistent with ion Doppler spectroscopy (IDS) measurements that show low plasma flow velocities from the injectors into the spheromak.

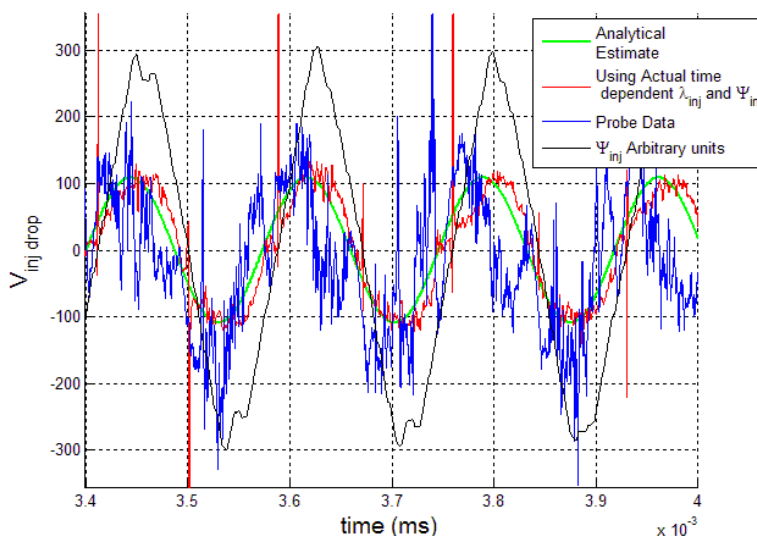


Figure 9. Blue curve: measured voltage drop in the x-injector as a function of time from Langmuir probe data for shot 106556. Red and green curves: calculations of the voltage drop needed to maintain only the injector helicity. Black curve: shape of the injector flux, for reference.

#### 4. Conclusion

Spheromaks with currents up to 29 kA have been formed and sustained in steady state using inductive helicity injection. The surface and internal magnetic probe data agree extremely well with the Taylor equilibrium. The amount of peak spheromak current and the threshold for spheromak formation are in agreement with helicity balance, further confirming the model. Langmuir probe and IDS data show helicity is injected into the spheromak from the insulated walls of the spheromak region and not from the “injectors”. Topics of continuing research include understanding the occasional flipping of the spheromak, understanding the decrease in sustained spheromak current with time, understanding the non-linear coupling of the odd symmetry injectors to the even symmetry spheromak, and understanding relaxation and its limitations for current drive applications.

#### 5. Acknowledgements

The Authors wish to thank Professor Masayoshi Nagata for the use of his IDS instrument and John Rogers and George Andexler for their technical assistance. This work is sponsored by the United States Department of Energy.

- 
- [1] Taylor J. B., Rev. Mod. Phys. **58**, 741 (1986).
  - [2] T. R. Jarboe et al., Phys. Rev. Lett., **97**, 115003 (2006).
  - [3] Sieck P. E. et al., IEEE Trans. Plasma Sci., **33**, 723 (2005).
  - [4] Sieck P. E. et al., Nuc. Fusion, **46**, 254 (2006).
  - [5] P. E. Sieck, PhD Thesis, University of Washington (2006).
  - [6] R. G. O’Neill et al., Phys. Plasmas **14**, 112304 (2007).
  - [7] R. Z. Aboul Hosn, Master Thesis, University of Washington (2007).
  - [8] R. G. O’Neill, PhD Thesis, University of Washington (2007).